EEET ECOLOGICAL ENGINEERING & ENVIRONMENTAL TECHNOLOGY

Ecological Engineering & Environmental Technology, 2026, 27(10), 96–117
https://doi.org/10.12912/27197050/231071
ISSN 2719–7050, License CC-BY 4.0

Received: 2026.07.27
Accepted: 2026.08.28
Published: 2026.09.10

Vulnerability analysis of coastal tidal flooding in Pekalongan City using composite mapping analysis method

Saptono Putro[1], Edi Kurniawan[1*], Mohammad Syifauddin[1], Visen Wijaya[1], Siti Nurindah Sari[2]

[1] Geography Department, Universitas Negeri Semarang, Indonesia
[2] Geography Education Study Program, Universitas Ivet, Indonesia
* Corresponding author's e-mail: edikurniawan@mail.unnes.ac.id

ABSTRACT

Coastal tidal flooding remains a major environmental hazard threatening the coastal areas of Pekalongan City, Indonesia. This study aims to analyze the spatial distribution of tidal flood vulnerability and identify the most influential driving factors affecting the coastal zone of Pekalongan City using the quantitative composite mapping analysis (CMA) method based on spatiotemporal data from 2022 to 2026. The analysis integrates seven environmental physical parameters: observed tidal flood inundation (derived from Sentinel-1 SAR imagery), Coastline buffer, River buffer, land subsidence, land cover (derived from Sentinel-2A imagery), elevation (National Digital Elevation Model/DEM Nasional), and rainfall (Climate Hazards Group InfraRed Precipitation with Station Data (CHIRPS). The validity of the digital modeling results was empirically verified through field observations and structured interviews conducted in the affected areas. The spatiotemporal analysis revealed considerable fluctuations in the extent of observed tidal flood inundation, covering 678 ha in 2022, decreasing to 525 ha in 2023 and 493 ha in 2024, reaching its lowest extent of 281 ha in 2025, before increasing sharply to 596 ha in 2026. The cumulative flood footprint totaled 810 ha, representing 17.54% of the entire study area. Ground-truth validation demonstrated a very high level of spatial agreement with the CMA model. The southern part of Pekalongan Utara District was confirmed as the most severely affected area, experiencing inundation depths reaching an adult's waist and flood durations of up to 10 days due to the combined effects of severe land subsidence and embankment failure. In contrast, the northern part of the district has experienced a marked reduction in flood frequency since the construction of a coastal seawall in 2022. This finding further demonstrates that the selected contemporary study period (2022–2026) provides an appropriate temporal basis for producing a near-real-time vulnerability map while minimizing bias associated with major structural interventions. These findings provide a robust scientific basis for local governments to establish priority strategies for disaster risk reduction and sustainable coastal management in Pekalongan City.

Keywords: coastal tidal flooding, disaster risk reduction, coastal areas, geographic information systems, composite mapping analysis.

INTRODUCTION

Coastal areas are highly dynamic environments that make substantial socio-economic contributions, particularly to the capture fisheries, brackish-water aquaculture, and coastal tourism sectors (Hapsoro and Buchori., 2015; Putro and Sriyono, 2021). The coastal zone of Pekalongan City, Central Java, is one of the region's key economic growth centers, supported by extensive aquaculture activities and coastal tourism destinations, including Sari Beach and Pasir Kencana Beach (Hudoyono., 2006; Triarso., 2012). However, the sustainability of human settlements and economic activities in this area is increasingly threatened by recurrent coastal tidal flooding (Wahjoerini, 2020; Brommer, 2009; Putro et al., 2024). Over recent decades, tidal flooding has evolved from a seasonal inundation event into a chronic environmental hazard that damages infrastructure, degrades environmental quality, and compels coastal residents to continually elevate their houses or even permanently relocate from areas that have become uninhabitable (Ismanto et al., 2021).

Recent environmental risk studies have emphasized that vulnerability in rapidly changing urban environments is determined by the interaction between biophysical processes and anthropogenic pressures rather than by isolated hazard factors alone (Millimono, 2026). This perspective highlights the need for integrated approaches capable of quantifying the combined effects of land deformation, hydrological connectivity, topographic conditions, and human-induced environmental changes in coastal flood assessment (Bale, 1994; Setyaningsih, 2021). The occurrence of tidal flooding in Pekalongan City is governed by complex interactions between natural physical processes and anthropogenic factors. While tidal fluctuations constitute the primary source of marine inundation, progressive land subsidence has emerged as the principal factor accelerating the spatial expansion and severity of flooding. The conversion of coastal land into densely populated residential areas and industrial zones has intensified excessive groundwater extraction, resulting in rapid ground deformation. In several locations, these conditions are further aggravated by river overflow and intense daily rainfall, whose discharge is impeded by tidal backwater effects, creating a compounding hazard that prolongs inland inundation (Pratama, 2019; Salim and Siswanto, 2021; Putra and Marfai, 2012). Furthermore, the temporal variability of climatic conditions is increasingly recognized as an important component in environmental risk assessment, particularly for hazards influenced by changing meteorological patterns (Odiana and Yusuf, 2026). Therefore, incorporating rainfall variability into coastal flood vulnerability assessments is essential for understanding compound flooding processes driven by the interaction between marine and atmospheric factors (Hutabarat, 2017; Sarah et al., 2021). Although the government has constructed seawalls and pumping systems to mitigate these impacts, several critical areas in Pekalongan Utara and Pekalongan Barat continue to experience recurrent flooding (Ibrahim, 2024).

Developing effective and sustainable coastal adaptation strategies requires accurate mapping of the spatiotemporal distribution of tidal flood vulnerability (Mutiarawati and Sudarmo, 2021; Putro and Hayati, 2007). Geographic information systems (GIS) and remote sensing provide a robust framework for modeling this type of hazard (Putro and Amira, 2024). Conventional flood-mapping approaches have generally relied on projections of the highest tidal level or static elevation models, which are insufficient for capturing the rapid environmental changes occurring from year to year. Recent advances in environmental monitoring have demonstrated the importance of continuous observation systems and data-driven approaches for improving the reliability of environmental assessment and supporting evidence-based decision-making (Oladosu et al., 2026). In this context, the integration of multi-temporal remote sensing observations provides an opportunity to capture dynamic environmental changes and improve the representation of evolving coastal flood conditions. Furthermore, standard overlay techniques commonly employ subjective scoring systems that fail to account for the actual relative importance of individual environmental parameters based on empirically observed flood conditions (Muttaqin et al., 2023; Setyaningsih et al., 2024; Putro et al., 2015).

To address the limitations of existing static flood models and subjective weighting approaches, this study evaluates contemporary tidal flood vulnerability in Pekalongan City post-2022 coastal seawall construction by integrating multi-temporal Sentinel-1 SAR observations, spatial environmental parameters, and composite mapping analysis (CMA). We hypothesize that land subsidence remains the dominant physical process governing flood persistence, that satellite-derived flood footprints provide an objective basis for parameter weighting, and that subsidence zones with disrupted hydraulic connectivity remain highly vulnerable despite coastal protection. Accordingly, this research aims to quantify the relative contributions of physical drivers and refine the understanding of mechanisms sustaining coastal tidal flooding under ongoing environmental transformation.

BACKGROUND

GIS-based monitoring of coastal tidal flooding

Historical flood change detection analysis plays a crucial role in understanding the spatial expansion of hydrometeorological hazards in coastal regions (Budiarto and Bioresita, 2023). In contemporary geographical studies, land cover refers to the observable physical characteristics of the Earth's surface, such as Water Body, vegetation, and bare land (Kasanah, 2020). In contrast, land use emphasizes the functional utilization of land by human activities, including residential areas, industrial zones, and agricultural land (Bunga et al., 2025; Jabbar and Handiani, 2023). Monitoring these spatial changes is essential because uncontrolled land-use conversion in coastal areas often reduces the natural water retention capacity of the land surface, thereby increasing surface runoff and prolonging inundation during high-tide events (Malik et al., 2023).

In many developing countries, conventional assessments of coastal vulnerability still rely heavily on field surveys, which are both time-consuming and costly (Wang et al., 2024). These limitations underscore the importance of GIS and remote sensing as alternative geospatial platforms capable of providing rapid, efficient, and large-scale spatial information. The integration of these technologies enables researchers to extract tidal inundation boundaries from high-resolution satellite imagery through multi-temporal analysis (Erkamim et al., 2023; Al-Omari et al., 2024)). Using composite analysis and post-classification comparison techniques, the spatial propagation of tidal flooding and changes in urban land-use sensitivity can be mapped in detail, thereby supporting disaster risk reduction-oriented spatial planning and policy formulation (Revathi et al., 2026).

Dynamics of coastal tidal flooding and land subsidence in coastal areas

Coastal tidal flooding is the inundation of low-lying coastal land by seawater during periods of high tide. Globally, this hazard is no longer viewed solely as a consequence of periodic tidal fluctuations or global sea-level rise but is increasingly recognized as the result of multiple interacting physical hazards (Egaputra et al., 2022). Among the geological factors contributing to this process, progressive land subsidence has been identified as one of the most significant drivers sustaining and accelerating the expansion of tidal inundation in low-lying coastal cities (Cao et al., 2021).

Land subsidence is primarily driven by a combination of natural processes, such as the consolidation of young sediments, and anthropogenic factors, particularly structural loading from dense urban development and excessive groundwater extraction for domestic and industrial purposes (Rizky, 2024). As land elevation continuously declines over time, the affected areas gradually develop geomorphological depressions that fall below mean sea level. This process creates substantial hydraulic disturbances, allowing seawater to penetrate farther inland through river channels and urban drainage networks. Moreover, land subsidence traps tidal water within these depressions, preventing efficient drainage back to the sea even after tidal levels recede, thereby substantially increasing the long-term vulnerability of coastal settlements (Juwono and Subagiyo, 2017).

The role of objective spatial methods in coastal disaster risk modeling

In conventional flood vulnerability modeling, the importance weights assigned to individual environmental parameters are often determined subjectively by researchers or derived from qualitative expert judgment through group discussions. Such approaches have inherent methodological limitations, including a high potential for personal bias and a limited ability to accurately represent the actual contribution of each environmental parameter to empirically observed flood events (Judijanto et al., 2024). To address these limitations, objective multicriteria analysis methods, such as CMA, have been developed. This objective spatial approach utilizes field-verified disaster occurrence points (ground truth) together with historical flood footprint polygons extracted from satellite imagery as the primary basis for mathematical weighting (Lasaiba, 2023; Koenawan and Zulfikar, 2025; Dewi and Syahra, 2025). Rather than assigning criterion scores and weights subjectively at the outset, CMA calculates them automatically according to the proportional area and spatial concentration of observed flood events within each parameter class. By integrating spatiotemporal environmental parameters with empirically derived flood footprints, the method produces contemporary flood vulnerability maps with high spatial accuracy while minimizing overestimation bias, thereby providing a reliable scientific basis for long-term disaster mitigation planning (Ran et al., 2018).

METHODOLOGY

Study area and spatial data sources

This study was conducted in Pekalongan City, Indonesia. Geographically, the study area consists predominantly of low-lying terrain with elevations ranging from 0 to 12 m above mean sea level. This relatively flat topography makes the area highly susceptible to tidal seawater intrusion and freshwater runoff from the surrounding river network.

The study adopts a multi-parameter spatial approach. All environmental parameters were derived from a combination of satellite remote sensing data and meteorological observations collected over a five-year period (2022-2026). The datasets comprise historical tidal flood records, spatial datasets, and satellite imagery. The data sources used in this study are summarized in Table 1.

To process, analyze, and synthesize these multi-source spatial datasets, a unified geospatial workflow was implemented using cloud computing platforms and GIS software covering the 2022–2026 observation period. Primary radar and optical satellite preprocessing, including Sentinel-1 SAR change detection and Sentinel-2 Random Forest land cover classification, were executed within GEE and the Sentinel Application Platform (SNAP). Secondary spatial layers, vector buffering, Kriging interpolations, and final vulnerability map visualizations were conducted using ArcGIS. The specific analytical procedures utilized to extract and standardize each of the seven spatial parameters are detailed as follows:

Tidal flood inundation

Spatiotemporal flood inundation footprints covering the 2022–2026 observation period were extracted from dual-polarization (VH) Sentinel-1A synthetic aperture radar (SAR) ground range detected (GRD) imagery operating in interferometric wide (IW) swath mode within GEE. Preprocessing involved establishing baseline reference images (before) and event inundation images (after) clipped to the study area geometry. To eliminate inherent radar speckle noise while preserving fine spatial edges and structural boundaries, an edge-adaptive Refined Lee directional speckle filter (7 × 7 window size) was applied by converting decibel values to linear natural units, executing directional filtering, and transforming the filtered backscatter intensity back to decibels (σ^0 in dB) (Singh et al., 2024).

$$Ri = \frac{\sigma\, vv\, (Flood)}{i\sigma\, vv\, (Preflood)} \tag{1}$$

where: Ri – rasio image, σ *vv* (*Flood*) – backscatter coefficient during or immediately after the flood event, *iσ vv* (*Preflood*) – backscatter coefficient before the flood event (baseline reference).

Actual inundation extent was delineated based on physical microwave scattering behavior over smooth water surfaces. Under cross-polarization (VH), open water bodies exhibit specular reflection that directs radar microwave signals away from the satellite sensor, yielding extremely low backscatter intensity values ($\sigma^0 < -20$ dB) (Twele et al., 2016). In contrast, non-flooded terrestrial land cover types produce significantly higher backscatter intensities ($\sigma^0 > -20$ dB) due to diffuse and volume scattering mechanisms. The backscatter threshold of –20 dB was selected as an optimal cutoff value because it effectively separates inundated pixels from dry land surfaces while remaining safely above the Noise Equivalent Sigma Zero (NESZ) floor (~ –22 dB) of the Sentinel-1 SAR instrument (Twele et al., 2016).

Consequently, pixels were classified as newly inundated flood zones if their baseline

Table 1. Data sources for CMA parameters

No.	Data	Data type	Data source
1.	Tidal flood inundation	Sentinel-1SAR GRD	ESA Copernicus
2.	Coastline buffer	Indonesian Base Map (*Rupa Bumi Indonesia)*	Geospatial Information Agency (BIG)
3.	River buffer	Indonesian Base Map (*Rupa Bumi Indonesia)*	Geospatial Information Agency (BIG)
4.	Land subsidence	Sentinel-1SAR SLC	ESA Copernicus
5.	Land cover	Sentinel-2A imagery	ESA Copernicus
6.	Elevation	National Digital Elevation Model (DEMNAS)	Geospatial Information Agency (BIG)
7.	Rainfall	Rainfall intensity	CHIRPS

backscatter intensity exceeded the threshold ($\sigma^0_{\text{preflood}} > -20\ \text{dB}$) while dropping below it during the inundation event ($\sigma^0_{\text{flood}} < -20\ \text{dB}$). Conversely, permanent waterbodies were isolated where backscatter values remained consistently below the threshold ($\sigma^0_{\text{preflood}} < -20\ \text{dB}$ and $\sigma^0_{\text{flood}} < -20\ \text{dB}$). The resulting binary flood mask was multiplied by individual pixel areas (m^2) to calculate total inundation surface area in hectares (ha) at a spatial resolution of 10 meters and exported for spatial overlay integration.

Coastline buffer

Coastline proximity was evaluated using vector spatial buffering applied to the high-precision shoreline layer (SHP format) obtained from the Geospatial Information Agency (Badan Informasi Geospasial – BIG), updated with high-resolution optical satellite imagery. Spatial processing was executed in ArcGIS software using the Buffer analytical tool to generate multi-ring proximity zones landward from the coastline. The vector buffer zones were subsequently converted into raster format to model the physical attenuation of marine wave action, storm surge energy, and direct tidal overflowing toward inland areas.

River buffer

Spatial exposure to riverine backwater effects and fluvial flooding was processed using vector spatial buffering along primary and secondary drainage networks. The drainage layer was extracted from the official vector base map dataset (SHP format) obtained from the Geospatial Information Agency (Badan Informasi Geospasial – BIG). Spatial processing was executed in ArcGIS software using the Buffer analytical tool to construct multi-ring proximity zones surrounding active river channels. The resulting vector buffer layers were subsequently converted into raster format to model the spatial gradient of high-tide backwater retention, where incoming ocean tides impede upstream river discharge and exacerbate riparian flood exposure.

Land subsidence

Annual land subsidence velocity maps (cm/year) covering the 2022–2026 observation window were derived from time-series Persistent Scatterer Interferometry Synthetic Aperture Radar (InSAR) processing using Sentinel-1 C-band Single Look Complex (SLC) imagery operating in interferometric wide (IW) swath mode. A total of 120 multi-temporal Sentinel-1 scenes were processed in the SNAP. Interferometric processing within SNAP involved precise orbit application, S1-TOPS coregistration using back-geocoding, interferogram formation, and topographic phase removal utilizing the 30-meter Copernicus DEM. Stable Persistent Scatterer (PS) target points were identified based on a temporal coherence threshold (>0.75) and amplitude dispersion analysis ($D_A < 0.25$). Spatiotemporal filtering was applied to estimate and remove Atmospheric Phase Screen (APS) artifacts, achieving an estimated vertical displacement accuracy of ± 2.5 mm/year root mean square error (RMSE). The extracted line-of-sight (LOS) displacement measurements were converted into vertical deformation velocity vectors.

Land cover classification

LULC dynamics were mapped using multi-temporal Sentinel-2 Surface Reflectance imagery (COPERNICUS/S2_SR_HARMONIZED) acquired over the 2026 observation period within the GEE cloud platform. To obtain a high-quality cloud-free surface reflectance composite, scene filtering was restricted to images with cloudy pixel percentages under 15%, followed by bitwise QA60 cloud and cirrus masking. A temporal median composite was subsequently generated across the study area. Supervised land cover classification was executed at a 10-meter spatial resolution using a Random Forest (RF) machine learning ensemble classifier consisting of 100 decision trees (smileRandomForest(100)). The classifier was trained on empirical ground-truth polygon samples digitised across the study area using six core spectral bands as input predictors: B2 (Blue), B3 (Green), B4 (Red), B8 (Near-Infrared), B11 (Short-Wave Infrared 1), and B12 (Short-Wave Infrared 2). The landscape was categorized into five distinct primary LULC classes: water body, built up land, open land, agriculture, and vegetation. The resulting classified raster was exported as a GeoTIFF at 10-meter resolution for spatial overlay and integration within ArcGIS software (Breiman, 2001; Congalton and Green, 2019).

Elevation processing

Topographic elevation (meters above sea level) was extracted from the National Digital Elevation Model (DEMNAS) integrated with 30-meter Copernicus DEM datasets. Hydrological preprocessing was executed in ArcGIS software using spatial analysis tools to fill artificial sinks and enforce continuous surface drainage routing across low-lying coastal terrains. The processed elevation raster was subsequently reclassified within ArcGIS into continuous topographic classes to model gravity-impeded drainage conditions and spatial susceptibility to astronomical high tides.

Rainfall intensity

Annual precipitation intensity (mm/year) covering the 2022–2026 observation period was derived from gridded Climate Hazards Group InfraRed Precipitation with Station data (CHIRPS) and validated using observation records from local BMKG meteorological stations. Spatial interpolation was executed in ArcGIS software using the Kriging deterministic/geostatistical method to construct a continuous annual rainfall intensity raster surface. The resulting precipitation layer was then reclassified within ArcGIS to assess the spatial variation of pluvial runoff contributions across the study area.

Composite mapping analysis (CMA) method

All environmental parameters were integrated and modeled using the CMA algorithm. Unlike conventional linear overlay methods, which commonly assign parameter weights subjectively, CMA automatically determines the weight of each criterion according to its spatial correlation with observed tidal flood footprint polygons identified from empirical data (Ran, 2018). The mathematical formulation used to calculate the flood vulnerability index (FVI) Index for each spatial pixel is expressed as follows:

$$FVI = \sum_{i=1}^{n}(Wi + Xi) \quad (2)$$

Wi is formulated as follows.

$$Wi = \frac{Mi}{\Sigma Mi} \quad (3)$$

Xi is formulated as follows.

$$Xi = \left(\frac{Oi}{Ei}\right) \cdot \frac{100}{\sum(Oi/Ei)} \quad (4)$$

where: *FVI* – flood vulnerability index, *Wi* – weight of the i-th parameter, *Xi* – score of the i-th parameter class, *Mi* – area of the parameter, *Oi* – number of observed flood occurrences, *Ei* – expected number of flood occurrences.

The parameter weights (W) were determined objectively by calculating the proportional contribution of each environmental parameter to the total delineated flood area. Based on the CMA matrix calculation, land subsidence was identified as the dominant controlling factor. The resulting FVI values were subsequently classified within a Geographic Information System to generate flood vulnerability zonation consisting of five levels: Very Low, Low, Moderate, High, and Very High.

Field validation

Field validation was conducted to evaluate the accuracy of the digital spatial model generated by the CMA algorithm through a systematic ground-truth survey across five affected urban villages (*kelurahan*). The survey combined terrestrial spatial observations with structured interviews involving local residents directly impacted by tidal flooding. Primary field data collection focused on three key indicators: (1) the maximum spatial extent of flood inundation, (2) actual inundation depth measured using field instrumentation within residential areas, and (3) the duration of floodwater retention alongside local drainage infrastructure conditions. Concurrently, in-depth community interviews were conducted to obtain historical information regarding shifts in flood frequency over time, with particular emphasis on conditions before and after the coastal seawall became operational in 2022.

To evaluate the spatial fidelity of the CMA model, field validation was conducted on May 10–11, 2026, using 30 empirical ground-truth verification points recorded via GPS receivers within high and very high vulnerability zones. A targeted purposive sampling strategy was employed, explicitly focusing on high-risk urban residential sectors and active inundation zones. In spatial hazard mapping, targeting verification points toward specific flood footprints is methodologically optimal to verify inundation boundaries, as unconstrained random sampling across large non-flooded terrains yields low diagnostic value regarding flood detection accuracy (Foody, 2002; Congalton and Green, 2019). Furthermore, establishing 30 empirical validation points aligns with the established statistical rule of thumb requiring 20 to 30 sample points per feature class to reliably quantify spatial accuracy without compromising field survey efficiency (Congalton, 1991; Jensen,2015).

Field validation was conducted on May 10–11, 2026, using 30 empirical ground-truth verification points recorded via GPS receivers. Initially, these 30 observation points were collected across high-risk urban residential sectors and active inundation zones as an initial baseline validation to verify the empirical flood footprint and inundation boundaries. Targeting verification points toward specific flood footprints is methodologically optimal for confirming actual inundation extent, as unconstrained random sampling across non-flooded terrains yields low diagnostic value regarding flood detection accuracy (Foody, 2002; Congalton and Green, 2019). Furthermore, establishing 30 empirical validation points aligns with established statistical standards requiring 20 to 30 sample points to reliably quantify spatial accuracy without compromising field survey efficiency (Congalton, 1991; Jensen, 2015).

Building upon this initial flood footprint verification, a balanced testing subset of 20 verification points was selected from the field observation locations to evaluate the multi-class spatial fidelity of the CMA model across all risk levels without calibration bias. Following good practice recommendations for spatial accuracy assessment (Stehman, 2009; Olofsson et al., 2014), the sampling was stratified equally across all five vulnerability tiers (Very Low, Low, Moderate, High, and Very High; n = 4 per class). This equal-stratification design prevents class-imbalance bias during accuracy assessment. Model performance was quantified using a multi-class confusion matrix, deriving overall accuracy, producer's accuracy, user's accuracy, and class-specific F1-scores.

Uncertainty and sensitivity analysis

To evaluate the impact of input data errors and spatial variations on the final tidal flood vulnerability map, an uncertainty analysis was performed comprising parameter sensitivity testing, CMA weight robustness checks, and spatial resolution harmonization (Lodwick et al., 1990; Saltelli et al., 2008). A single-parameter sensitivity analysis and weight perturbation tests (±10% to ±20% variance)

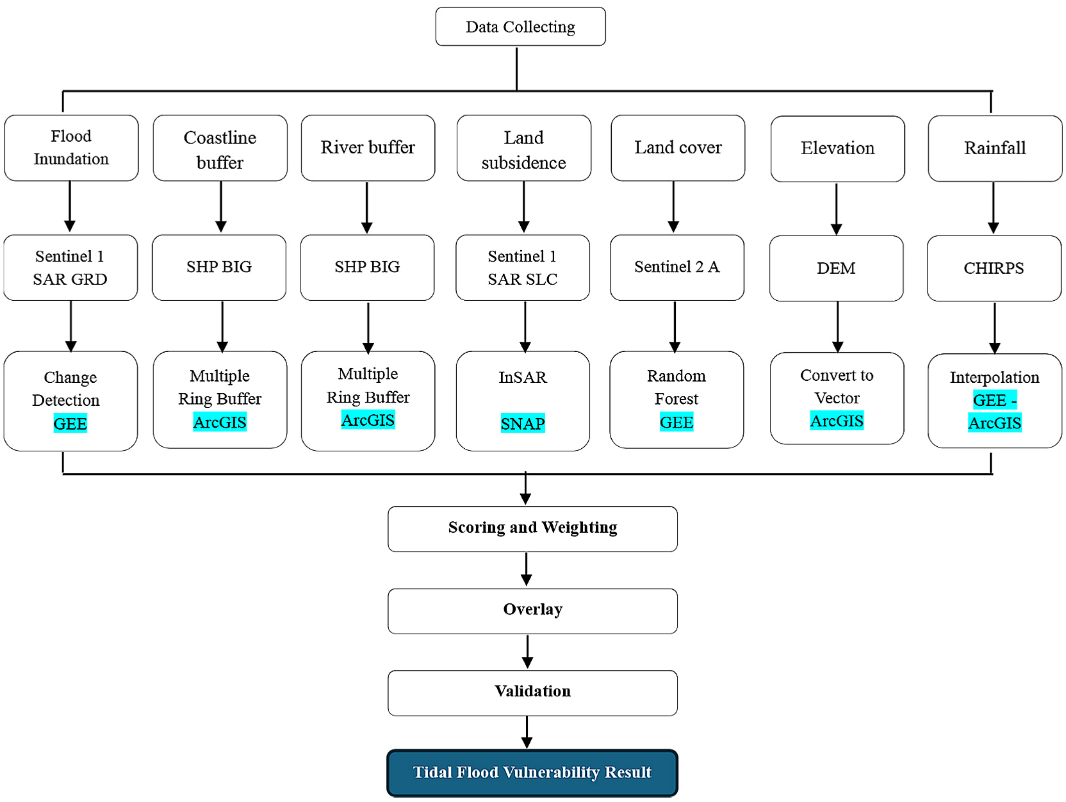

Figure 1. Temporal detection of tidal flood inundation

were applied to the CMA criteria weights, revealing that land subsidence and elevation exerted the highest spatial influence while maintaining structural model stability across vulnerability classes (Feizizadeh and Blaschke, 2013). Additionally, to address the spatial resolution mismatch between high-resolution raster layers (Sentinel-1 SAR at 10 m and Copernicus DEM at 30 m) and coarser precipitation grids (CHIRPS at ~5 km), all environmental criteria were resampled and aligned to a standardized 10-meter spatial grid using bilinear interpolation in ArcGIS prior to spatial overlay (Atkinson, 2013). This multi-resolution harmonization effectively minimized cell boundary aggregation errors along low-lying coastal margins.

Flowchart

The overall methodological workflow for evaluating tidal flood vulnerability is systematically illustrated. The spatial analytical framework integrates multi-source datasets including Sentinel-1 SAR, Sentinel-2A, SHP BIG vector layers, DEM, and CHIRPS precipitation processed across Google Earth Engine (GEE), ESA SNAP, and ArcGIS platforms. The workflow progresses from primary satellite image processing and GIS spatial operations to criteria scoring, weighted spatial overlay, and empirical field validation to derive the final tidal flood vulnerability map (Figure 1).

RESULTS AND DISCUSSION

Results

Spatiotemporal distribution of observed tidal flood inundation (2022–2026)

The spatial and temporal distribution of observed tidal flood inundation in the coastal area of Pekalongan City was identified using Google Earth Engine through the processing of Sentinel-1 SAR imagery (Pande, 2022). Based on changes in radar backscatter coefficients analyzed using the Change Detection method, the annual extent of tidal flood inundation exhibited a fluctuating pattern throughout the five-year observation period.

In 2022, the extent of tidal flood inundation in Pekalongan City reached 678 ha, indicating a relatively widespread flooding event. The inundated area subsequently declined over the following two years, decreasing to 525 ha in 2023 and further to 493 ha in 2024. The most pronounced reduction occurred in 2025, when the inundated area reached its minimum extent of 281 ha. From a hydrological perspective, this gradual decline suggests the increasing effectiveness of flood-control infrastructure, including floodgates, pumping systems, and the large coastal seawall, all of which began operating optimally toward the end of 2022.

To evaluate the impact of coastal infrastructure and short-term environmental drivers, the temporal dynamics of inundation space were analyzed across the observation period. Inter-annual and seasonal SAR change detection comparisons revealed distinct spatial shifts in flood footprints following localized seawall construction and coastal dike maintenance. Prior to structural completion, tidal floodwaters penetrated deeper into urban residential sectors and agricultural land. Following infrastructure consolidation, surface inundation became restricted to low-lying peripheral zones, demonstrating the localized effectiveness of protective barriers against astronomical high tides, despite ongoing regional land subsidence pressures. Nevertheless, a substantial increase in inundation extent occurred in 2026, when the flooded area expanded sharply to 596 ha. This anomalous increase was primarily

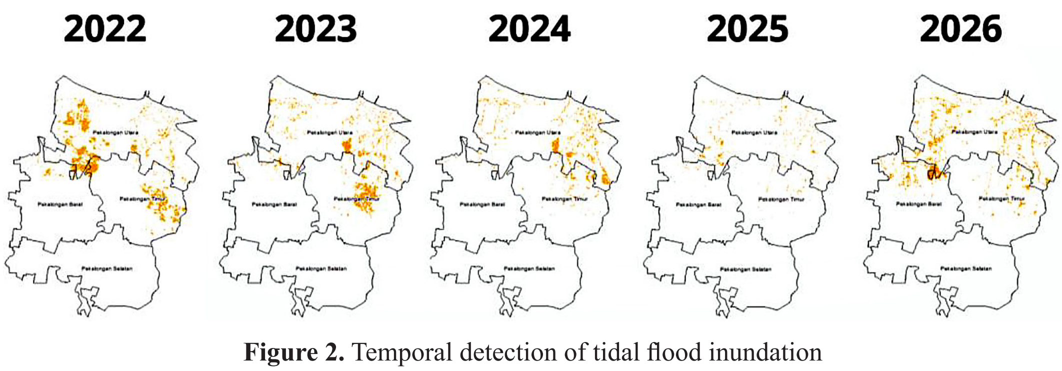

Figure 2. Temporal detection of tidal flood inundation

associated with extreme meteorological conditions characterized by exceptionally high cumulative daily and monthly rainfall coinciding with the annual spring tide, which generated extensive inland water accumulation as upstream river discharge was unable to drain effectively into the sea. By integrating the annual inundation maps into a composite temporal flood footprint, the cumulative extent of observed tidal flooding in Pekalongan City during the 2022–2026 period was estimated at 810 ha, equivalent to 17.54% of the total study area (Figures 2, 3).

CMA-based vulnerability assessment and parameter scoring

The following sections present the detailed results of the objective CMA matrix calculations for each environmental parameter used to determine tidal flood vulnerability in Pekalongan City.

Flood inundation parameter

This parameter was used to evaluate the internal consistency of the vulnerability model. The empirical field verification yielded high spatial agreement between the CMA model predictions and observed ground conditions. Out of the 30 targeted validation points, 29 points demonstrated direct conformity with actual flood inundation occurrences, while 1 point exhibited a minor localized anomaly. Specifically, 29 of the 30 validation points were located within the Inundated class (810 ha), yielding a theoretical expected value of 5.26 and an observed to expected (O/E) ratio of 5.51, resulting in a high CMA score of 0.99. In contrast, the Non inundated class (3.809 ha) contained only one observed flood occurrence, with an expected value of 24.74 and an O/E ratio of 0.04, producing the lowest score (0.01). Overall, these results demonstrate that the satellite derived temporal inundation delineation exhibits a very high degree of spatial agreement with actual flood conditions observed in the field (Figure 4).

Coastline buffer

Coastline buffer was derived using a buffer-based zonation approach. The CMA matrix analysis showed that the 500-m buffer achieved the highest score (0.323), with three observed flood occurrences within an area of 131.92 ha. The 750-m buffer ranked second with a score of 0.312 (three flood occurrences; 136.53 ha), followed by the 1.000-m buffer, which scored 0.193 (two flood occurrences; 147.23 ha). The 250-m buffer

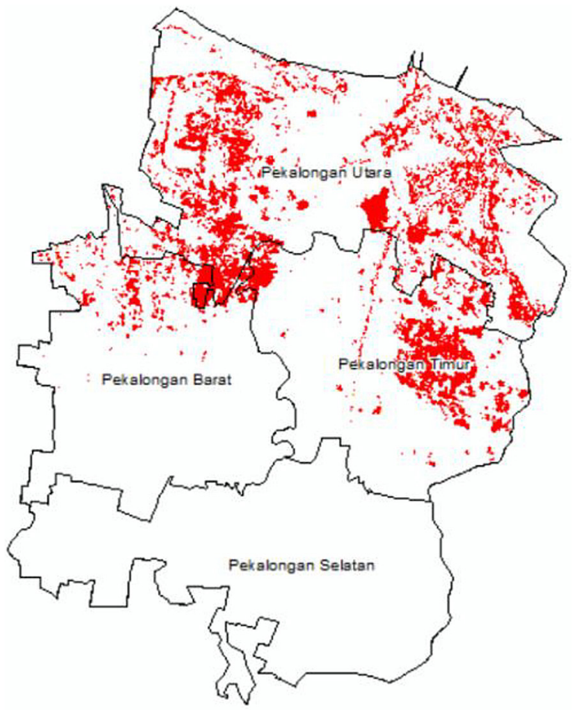

Figure 3. Cumulative tidal flood footprint

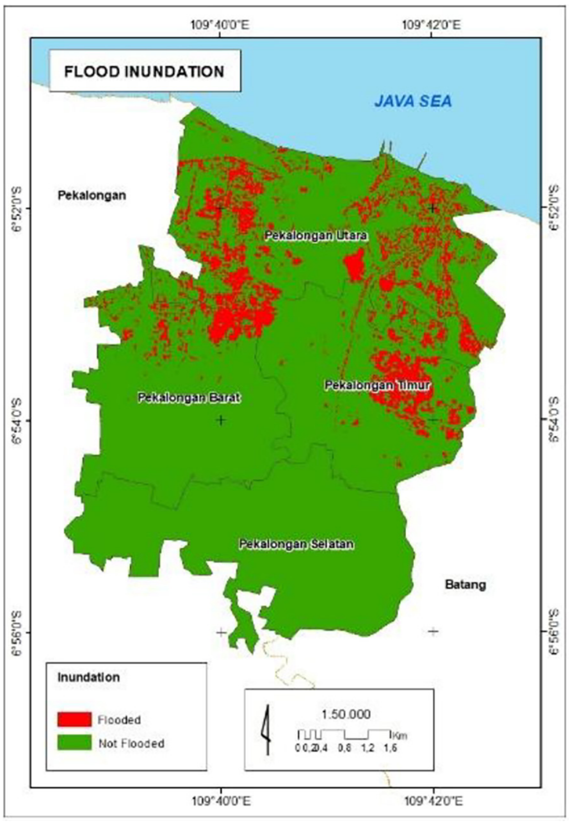

Figure 4. Flood inundation

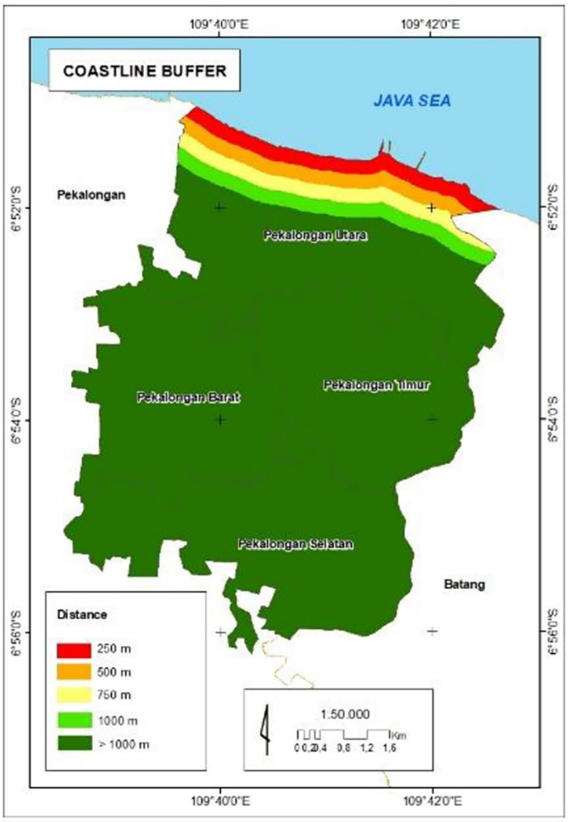

Figure 5. Coastline buffer

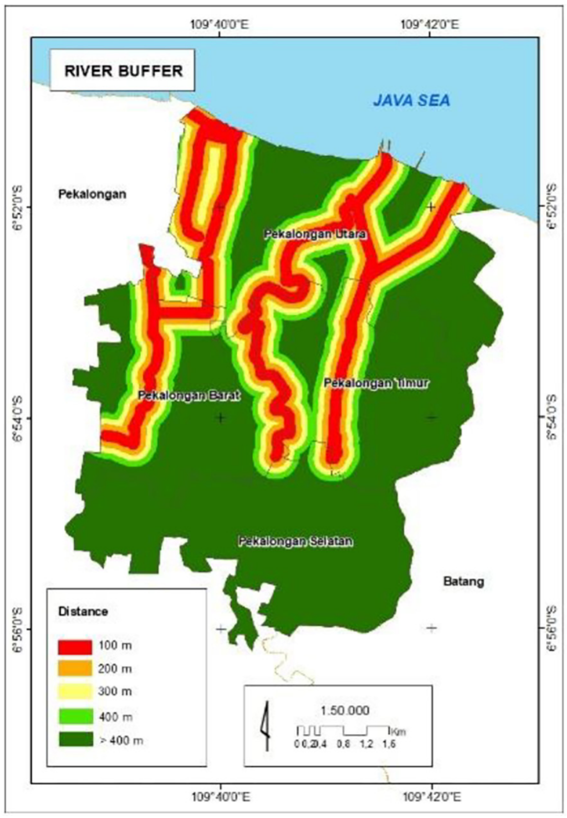

Figure 6. River buffer zones

obtained a score of 0.099 (one flood occurrence; 143.14 ha), while areas located more than 1.000 m from the coastline recorded the lowest score (0.073). Although this class contained 21 flood occurrence points, its considerably larger area (4,059.90 ha) reduced its relative vulnerability score (Figure 5).

River buffer

Rivers function as the principal hydraulic corridors that convey tidal seawater into inland residential areas. The CMA analysis confirmed that the most critical zone lies within 0–100 m of the riverbanks, which achieved the highest score (0.627). Although this zone covers only 549.76 ha, it contained five observed flood occurrence points. Vulnerability decreased progressively with increasing distance from the river. The 200-m buffer recorded a score of 0.153 (three flood occurrences), the 300-m buffer scored 0.057 (one flood occurrence), the 400-m buffer scored 0.066 (one flood occurrence), while areas located more than 400 m from rivers recorded a score of 0.097 despite containing 11 flood occurrence points distributed across a much larger area of 2,778.69 ha (Figure 6).

Land subsidence parameter

Ground deformation in the form of land subsidence was identified as the environmental parameter exerting the strongest spatial influence on tidal flooding in Pekalongan. Areas experiencing the highest subsidence rate (>0.300 m) contained 15 observed flood occurrence points within only 247.53 ha, resulting in the highest CMA score (0.772). Areas with subsidence rates between 0.121 and 0.300 m ranked second, with a score of 0.122 (four flood occurrences; 314.43 ha). Subsidence rates of 0.061–0.120 m produced a score of 0.071 (five flood occurrences; 899.54 ha). By contrast, areas exhibiting relatively stable ground conditions (0–0.021 m) recorded no observed flood occurrence points and therefore received a score of 0.000 (Figure 7).

Elevation parameter

Micro-topographic variation plays a critical role in controlling surface water retention. Low-lying areas with elevations between 0 and 1 m above mean sea level constitute natural water accumulation zones. Covering only 231.39 ha, this elevation class contained four observed flood

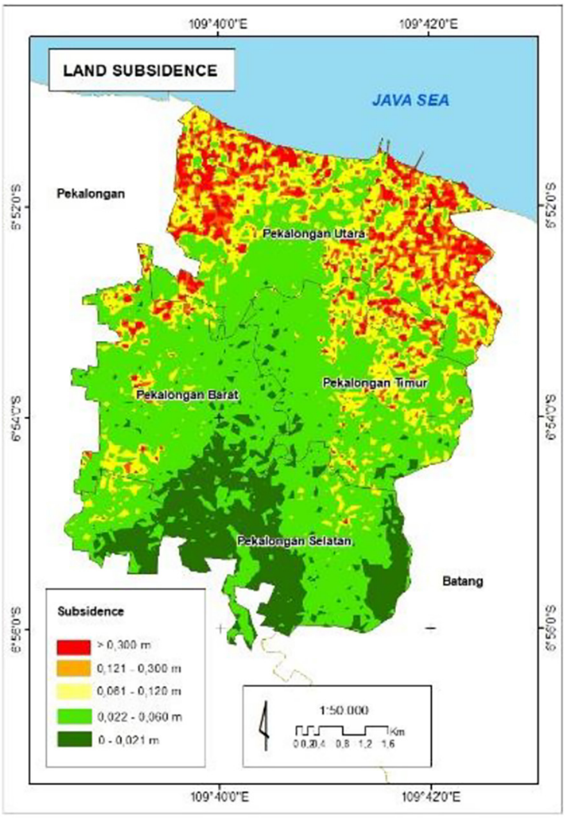

Figure 7. Land subsidence

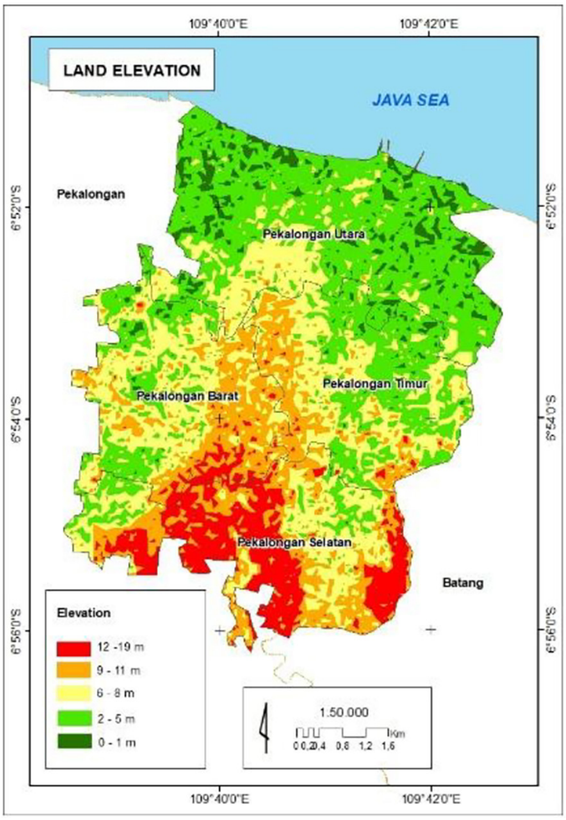

Figure 8. Land elevation

occurrence points and consequently received the highest CMA score (0.494). Vulnerability generally declined with increasing elevation. The 2–5 m elevation class recorded a score of 0.183 (11 flood occurrences; 1,715.93 ha), while the 6–8 m class scored 0.288 (14 flood occurrences; 1,387.05 ha). The 9–11 m class obtained a score of 0.035 (one flood occurrence; 825.15 ha), whereas upland areas between 12 and 19 m recorded a score of 0.000 because they were entirely beyond the influence of tidal inundation(Figure 8).

Land cover parameter

Land-cover characteristics reflect the sensitivity of different landscape types to tidal inundation. The CMA results identified Water Body as the most vulnerable land-cover class, receiving the highest score (0.354). Agriculture ranked second with a score of 0.138. Although Built-up Lands dominate land use within the city (1,626.64 ha) and contained a relatively high number of observed flood occurrences (eight points), their extensive spatial coverage resulted in a moderate CMA score of 0.130 (Figure 9).

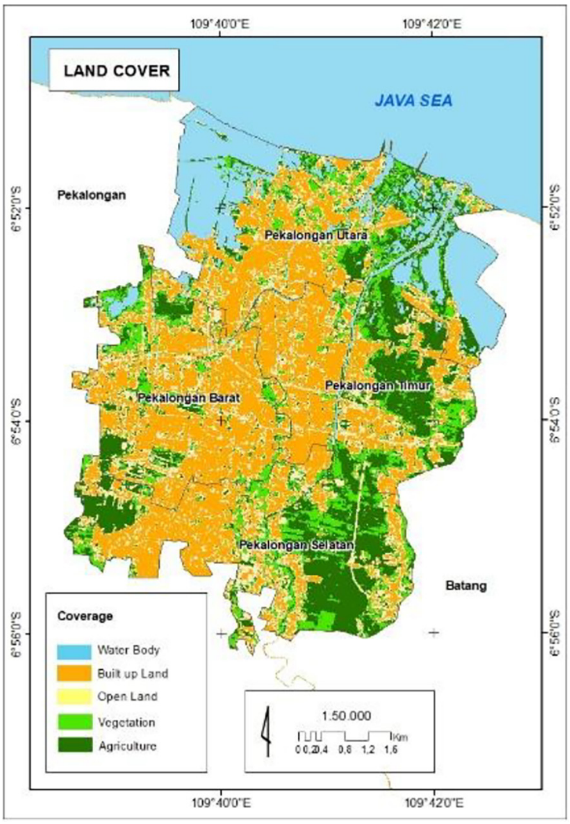

Figure 9. Land cover

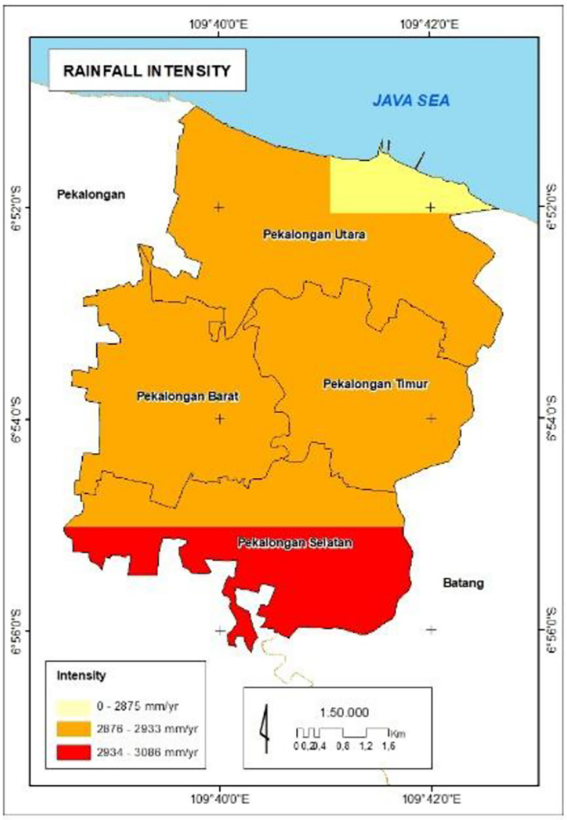

Figure 10. Rainfall intensity

Rainfall parameter

Rainfall acts as a meteorological factor that exacerbates tidal flood inundation by increasing surface water accumulation under restricted drainage conditions. The lowest rainfall class (0–2.875 mm year^{-1}) achieved the highest CMA score (0.67) because, despite covering only 204.30 ha, it precisely encompassed three observed flood occurrence points. In contrast, the 2.876–2.933 mm year^{-1} class dominated the study area, covering 3,728.40 ha and containing the majority of observed flood occurrences (27 points), resulting in a CMA score of 0.33. The highest rainfall class (2.934–3.086 mm year^{-1}) received a score of 0.00 because it did not intersect with any observed flood occurrence points (Figure 10, Table 2).

Parameter weighting

The spatial–temporal distribution of actual tidal flood inundation in the coastal area of Pekalongan City was identified using the Google Earth Engine platform through the processing of Sentinel-1 SAR imagery (Wang et al., 2024; Rizki, 2024). Based on the analysis of variations in radar backscatter coefficients using the change detection method (Kasanah, 2020), the extent of tidal flood inundation exhibited a fluctuating pattern throughout the five-year observation period.

After the score value (Xi) for each parameter class had been calculated, the final step of the CMA algorithm was to determine the parameter weight (Wi). These weights were derived objectively by dividing the cumulative Observed-to-Expected Ratio (O/E) of each parameter by the total cumulative O/E ratio of all seven physical environmental parameters included in the analysis (Ran et al, 2018).

Based on the calculations summarized in the CMA matrix, the cumulative O/E ratio of the seven parameters was 22.662. Using this objective normalization factor, the parameter weights and the relative contribution of each physical environmental factor to tidal flood vulnerability in Pekalongan City were calculated as follows (Table 3).

The objective weighting results clearly indicate that land subsidence (24.49%) and Coastline buffer (21.98%) are the two dominant factors controlling the spatial distribution and expansion of tidal flooding in Pekalongan City. River buffer (12.68%) and rainfall (6.85%) function as secondary hydrological and meteorological drivers, confirming the presence of a compounding hazard, whereby tidal inundation is intensified by river overflow and rainfall runoff that are prevented from discharging into the sea because of tidal backwater effects.

Tidal flood vulnerability

Overall, tidal flood vulnerability in Pekalongan City is dominated by relatively safe areas. The Very Low vulnerability class covers 2,528.52 ha (54.74%), extending across the upstream southern part of the city. The Low and Moderate vulnerability classes occupy 567.98 ha (12.30%) and 610.86 ha (13.23%), respectively, representing transitional geomorphological zones in the central part of the study area. In contrast, the critical vulnerability zones comprise 370.52 ha (8.02%) classified as High vulnerability and 541.12 ha (11.72%) classified as Very High vulnerability. These highly vulnerable areas are concentrated almost entirely in the northern and western parts of Pekalongan City, adjacent to the coastline and river estuaries (Figure 11, Table 4).

Table 2. CMA parameter calculations

Flood Inundation						
Class	Area (ha)	Area (%)	Observed flood points (O)	Expected flood points (E)	O/E	Score (Xi)
Inundated	810	17.54%	29	5.26	5.51	0.99
Non-inundated	3809	82.46%	1	24.74	0.04	0.01
Total	4619	100%	30	30	5.55	1
Coastline buffer						
Class	Area (ha)	Area (%)	Observed flood points (O)	Expected flood points (E)	O/E	Score (Xi)
250 m	143.14	3.10%	1	0.93	1.08	0.099
500 m	131.92	2.86%	3	0.86	3.50	0.323
750 m	136.53	2.96%	3	0.89	3.38	0.312
1000 m	147.23	3.19%	2	0.96	2.09	0.193
>1000 m	4059.9	87.90%	21	26.37	0.80	0.073
Total	4619	100%	30	30	10.85	1
Distance from the River						
Class	Area (ha)	Area (%)	Observed Flood Points (O)	Expected flood points (E)	O/E	Score (Xi)
100 m	549.76	11.90%	14	3.57	3.92	0.627
200 m	481.74	10.43%	3	3.13	0.96	0.153
300 m	433.73	9.39%	1	2.82	0.35	0.057
400 m	374.74	8.11%	1	2.43	0.41	0.066
>400 m	2778.69	60.16%	11	18.05	0.61	0.097
Total	4619	100%	30	30	6.26	1
Land subsidence						
Class	Area (ha)	Area (%)	Observed flood points (O)	Expected flood points (E)	O/E	Score (Xi)
0-0.021 m	652.92	14.14%	0	4.24	0.00	0
0.022–0.060 m	2504.28	54.22%	7	16.27	0.43	0.036
0.061–0.120 m	899.54	19.47%	5	5.84	0.86	0.071
0.121–0.300 m	314.43	6.81%	3	2.04	1.47	0.122
>0.300 m	247.53	5.36%	15	1.61	9.33	0.772
Total	4619	100%	30	30	12.09	1
Land cover						
Class	Area (ha)	Area (%)	Observed flood points (O)	Expected flood points (E)	O/E	Score (Xi)
Water body	596.71	12.92%	8	3.88	2.06	0.354
Built-up land	1626.64	35.22%	8	10.56	0.76	0.13
Open land	892.69	19.33%	3	5.80	0.52	0.089
Agriculture	957.57	20.73%	5	6.22	0.80	0.138
Vegetation	545.19	11.80%	6	3.54	1.69	0.29
Total	4619	100%	30	30	5.84	1
Land elevation						
Class	Area (ha)	Area (%)	Observed flood points (O)	Expected flood points (E)	O/E	Score (Xi)
0–1 m	231.39	5.01%	4	1.50	2.66	0.494
2–5 m	1715.93	37.15%	11	11.14	0.99	0.183
6–8 m	1387.05	30.03%	14	9.01	1.55	0.288
9–11 m	825.15	17.86%	1	5.36	0.19	0.035
12–19 m	459.18	9.94%	0	2.98	0.00	0
Total	4619	100%	30	30	5.39	1
Rainfall						
Class	Area (ha)	Area (%)	Observed flood points (O)	Expected flood points (E)	O/E	Score (Xi)
0–2875 mm/year	204.3	4.42%	3	1.33	2.26	0.67
2876–2933 mm/year	3728.4	80.72%	27	24.22	1.11	0.33
2934–3086 mm/year	686.01	14.85%	0	4.46	0.00	0
Total	4619	100%	30	30	3.38	1

Table 3. Weights of each parameter

Parameter	O/E (Mi)	Weight (Wi)	Weight (%)
Flood inundation	5.55	0.112439	11.24%
Coastline buffer	10.85	0.219814	21.98%
River buffer	6.26	0.126823	12.68%
Land subsidence	12.09	0.244935	24.49%
Land cover	5.84	0.118314	11.83%
Elevation	5.39	0.109198	10.92%
Rainfall intensity	3.38	0.068476	6.85%
Total (ΣM,ΣW)	49.36	1	100%

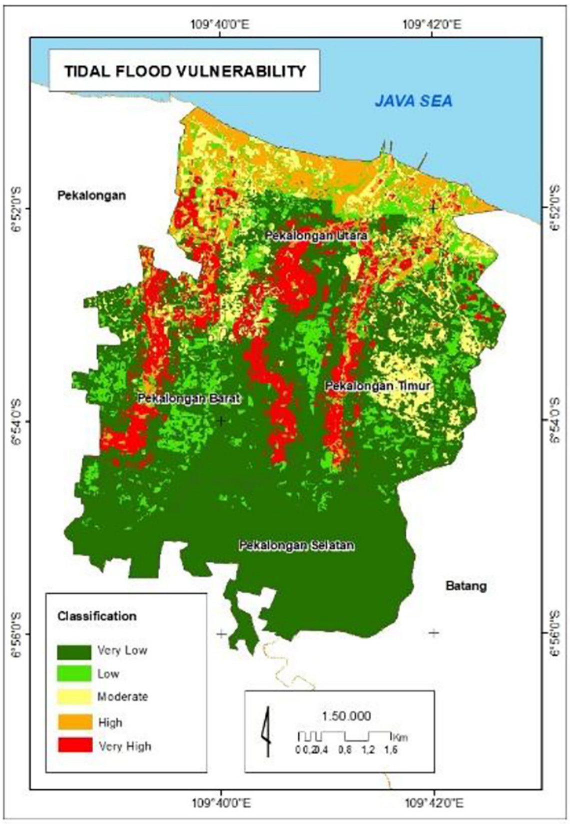

Figure 11. Tidal flood vulnerability map

Among all districts, Pekalongan Utara exhibited the highest level of vulnerability. It accounted for the largest proportion of the city's most critical vulnerability classes, comprising 237.57 ha classified as Very High vulnerability and 326.04 ha classified as High vulnerability within a total district area of 1,507.19 ha.

Pekalongan Barat ranked second in terms of vulnerability, containing 167.05 ha of Very High vulnerability and 23.74 ha of High vulnerability within a total area of 1,125.16 ha. Notably, the area classified as Moderate vulnerability (167.05 ha) was identical to that classified as Very High vulnerability, indicating a distinctive spatial distribution of flood susceptibility within the district.

Pekalongan Timur displayed a particularly heterogeneous spatial pattern, encompassing all five vulnerability classes across its 969.94-ha area. Although the district was predominantly characterized by the Very Low vulnerability class (566.16 ha) and the Low vulnerability class (118.35 ha), significant vulnerable zones were also identified, including 128.19 ha classified as Moderate, 20.74 ha as High, and 136.50 ha as Very High vulnerability.

In contrast, Pekalongan Selatan was identified as the least vulnerable district and was largely isolated from coastal hydrometeorological hazards. No areas were classified as Moderate, High, or Very High vulnerability. Instead, the district was overwhelmingly dominated by the Very Low vulnerability class (993.00 ha), with only a small proportion (23.71 ha) categorized as Low vulnerability, out of a total district area of 1,016.71 ha.

Sensitivity analysis of criterion weights

To evaluate the spatial stability and robustness of the CMA model outputs, a single-parameter sensitivity test was conducted on the primary physical driver, Land Subsidence (W = 24.49%). The weight of land subsidence was perturbed by ±10% (Scenario 1: ±10%, Scenario 2: –10%), while the remaining six parameter weights were re-normalized proportionally to preserve a strictly constant weight sum ($\sum W_i = 1.00$). The resulting area variations across vulnerability tiers are detailed and visualised in Figure 12.

The sensitivity analysis revealed minor and asymmetrical spatial area shifts across all vulnerability classes. Increasing the land subsidence

Table 4. Area and percentage of tidal flood vulnerability by district

District	Vulnerability area (ha)					District area (ha)
	Very high	High	Moderate	Low	Very low	
Pekalongan Utara	237.57	326.04	315.62	279.96	348	1507.19
Pekalongan Barat	167.05	23.74	167.05	145.96	621.36	1125.16
Pekalongan Timur	136.5	20.74	128.19	118.35	566.16	969.94
Pekalongan Selatan	-	-	-	23.71	993	1016.71
Total area	541.12	370.52	610.86	567.98	2528.52	4619
Percentage	12%	8%	13%	12%	55%	100%

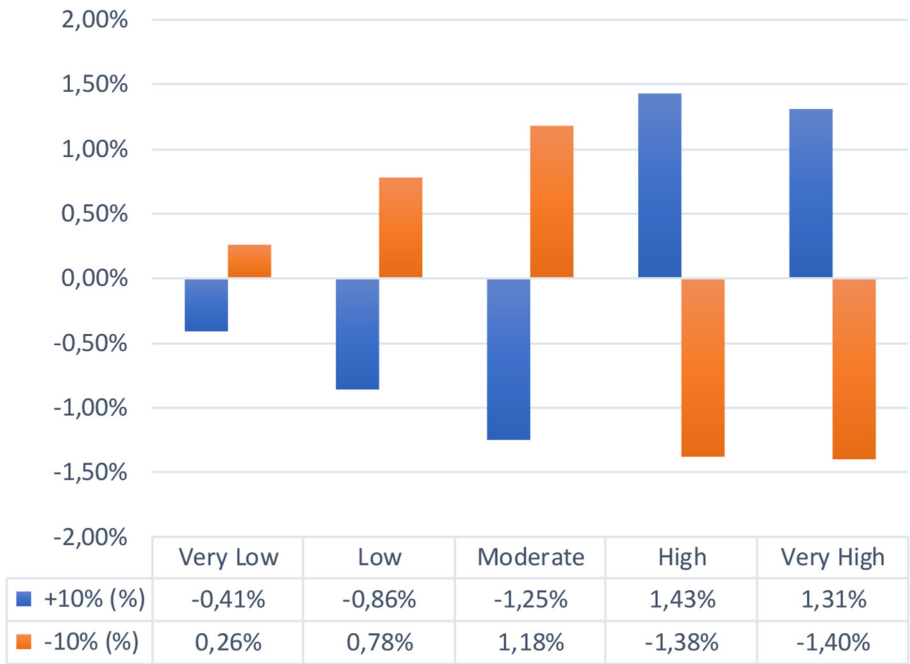

Figure 12. Tidal flood vulnerability map

weight (+10%) expanded the High and Very High vulnerability classes by +1.43% (+5.28 ha) and +1.31% (+7.08 ha), respectively, primarily absorbing area from the adjacent Moderate class (–1.25%). Conversely, decreasing the weight (-10%) reduced the High and Very High classes by –1.38% (–5.12 ha) and –1.40% (–7.60 ha).

Across all tested scenarios, the maximum area variation across all classes was strictly bounded within ±1.43%, while the total study area remained completely conserved (4,619.00 ha, 100%). According to established spatial MCDA sensitivity analysis benchmarks (Saltelli et al., 2008; Chen et al., 2010; Feizizadeh and

Table 5. Area and percentage of tidal flood vulnerability by district

Vulnerability class	Baseline area (ha)	Baseline (%)	Scenario 1: +10% (ha)	Scenario 2: -10% (ha)
Very Low	2.528,52	55%	2.518,20	2.535,10
Low	567,98	12%	563,12	572,4
Moderate	610,86	13%	603,2	618,1
High	370,52	8%	375,8	365,4
Very High	541,12	12%	548,2	533,52
Total Area	4.619,00	100%	4.619,00	4.619,00

Blaschke, 2013), a spatial model output is classified as highly stable if criterion weight perturbations within ±10% to ±20% induce class area shifts below the 5% threshold. Because the maximum observed shift in this study (≤ 1.43%) is significantly below this threshold, the resulting vulnerability map demonstrates exceptionally high spatial stability and robustness against parameter weight fluctuations (Table 5).

DISCUSSION

Comparison with previous studies

The spatiotemporal analysis of observed flood inundation provides fundamental insight into the persistence and evolution of areas directly affected by coastal hydrodynamic processes Putra and Marfai, 2012). The temporal modeling results, which revealed fluctuations in inundation extent from 678 ha to 596 ha over the study period, are consistent with the principles of coastal hydrology, whereby the cumulative flood footprint represents one of the most reliable indicators of the functional performance of urban drainage systems. This finding is also consistent with previous studies on flood management in Pekalongan (Salim and Siswanto, 2021). The incorporation of observed inundation data is therefore essential for minimizing spatial modeling bias, as many earlier coastal hazard assessments relied primarily on static tidal projections that failed to capture the evolving extent of actual inland inundation.

From a theoretical perspective, proximity to the coastline governs the degree of land exposure to marine hydrodynamic forces, particularly wave overtopping during high tides. Previous studies conducted along the northern coast of Java have consistently shown that areas closest to the shoreline exhibit the highest flood risk because of the absence of natural energy dissipation mechanisms (Setyaningsih, 2021). However, the empirical findings of this study reveal a different pattern in Pekalongan City. The immediate coastal zone exhibits relatively controlled vulnerability owing to the presence of a large-scale coastal seawall (Ibrahim et al., 2024). In contrast, areas lacking seawall protection, particularly those located adjacent to river channels, remain highly vulnerable because tidal water penetrates inland through river estuaries, providing alternative pathways for marine inundation.

The principal river network was also found to function as the primary hydraulic conduit transporting tidal water into inland residential areas. This spatial pattern is consistent with the coastal hydrodynamic theory of the backwater effect, whereby tidal hydrostatic pressure obstructs downstream river discharge and forces river water upstream. Consistent with previous urban hydrology studies, severe riverbed sedimentation further reduces channel capacity, accelerating river overflow beyond the riverbanks. This mechanism explains why settlements along the Meduri River experience substantially more severe inundation than settlements located directly along the open coastline.

Vertical ground deformation in the form of land subsidence was identified as the dominant geological factor controlling tidal flood vulnerability. This finding strongly supports previous studies conducted along the northern coast of Java, which have demonstrated that intensive groundwater extraction associated with industrial activities and densely populated urban areas accelerates the consolidation of young alluvial sediments (Hutabarat, 2017; Sarah et al., 2021; Rizki, 2024). The resulting land subsidence gradually forms geomorphological depressions (the bowl effect) below sea level, reducing the natural hydraulic gradient required for seawater to drain back into the sea after high tide. Consequently, tidal water remains trapped within these depressions, substantially prolonging flood duration in residential areas.

Micro-topographic variation, represented by land elevation, also plays a critical role in regulating surface water movement. Low-lying areas with elevations between 0 and 1 m above mean sea level function as natural storage basins for tidal inundation. The importance of this parameter supports the theoretical framework of digital elevation model (DEM)-based flood vulnerability analysis, whereby extremely gentle topographic gradients allow even centimeter-scale increases in sea level to propagate inundation several kilometers inland. In contrast, the higher-elevation southern part of the study area remains largely isolated from tidal influences.

Land-use configuration reflects the capacity of different landscapes to retain or convey floodwater. From the perspective of urban environmental geography, the conversion of wetlands and mangrove ecosystems into densely built, impervious urban areas substantially increases surface runoff coefficients (Pande, 2022). These findings are consistent with the theory of coastal urban sprawl, which suggests that inadequate consideration of local drainage capacity during urban expansion limits infiltration and drainage, thereby accelerating the accumulation of tidal floodwater on transportation infrastructure and within residential areas (Revathi et al., 2026).

Rainfall constitutes the principal meteorological driver contributing to the occurrence of compounding hazards in coastal environments. When intense local rainfall coincides with spring tides, urban drainage systems may experience complete hydraulic failure because tidal backwater prevents freshwater from discharging into the sea. These findings reinforce the contemporary disaster risk management perspective that coastal flooding in densely populated tropical cities should not be assessed solely as a marine hazard (Lasaiba, 2023). During high-tide conditions, flood-control gates and pumping systems are often unable to discharge stormwater effectively, resulting in prolonged freshwater inundation throughout urban areas.

Theoretical implications

Methodologically, while individual spatial overlay and satellite remote sensing techniques are widely established, the integration of multi-temporal Sentinel-1 SAR observations with CMA provides distinct advantages over conventional qualitative weighting frameworks in post-infrastructure coastal environments. A comparative benchmark against the conventional AHP method demonstrates the clear advantage of empirical weighting in the CMA framework. While both methods identify similar macro-level coastal risk clusters, AHP exhibits spatial overestimation along the immediate shoreline due to rigid linear criteria weighting. Validation using the independent field dataset confirms that CMA achieves higher predictive accuracy than AHP (95.00% vs. 85.00%. Overall Accuracy), successfully eliminating expert-derived subjectivity along transitional hazard boundaries.

Unlike the AHP, which relies heavily on subjective expert opinions that may introduce cognitive bias and fail to capture rapid environmental shifts (Malczewski and Rinner, 2015; Thammaboribal et al., 2025), the CMA algorithm objectively derives parameter weights directly from the spatial concentration of empirically observed flood footprints (De Vries et al., 2020; Xiao and Tang., 2018). By offering a transparent, physical-process-oriented, and data-driven weighting scheme, this framework accurately captures contemporary inundation dynamics following major structural interventions, such as the 2022 seawall construction in Pekalongan, while maintaining high spatial fidelity for local adaptation planning.

This study contributes to the advancement of disaster geography and multi-criteria spatial analysis using remote sensing by demonstrating the effectiveness of integrating the composite mapping analysis algorithm with multi-temporal Sentinel-1 radar imagery acquired between 2022 and 2026. The proposed framework strengthens the concept of objective hazard-footprint-based spatial weighting, replacing conventional qualitative weighting approaches based primarily on expert judgment with a data-driven mathematical procedure in which parameter weights are determined by the spatial concentration of empirically observed flood occurrences (Ran et al., 2018).

Furthermore, the findings expand the theoretical understanding of compounding hazards in low-lying tropical coastal environments. The study demonstrates that local geological processes (land subsidence), oceanographic forcing (tidal inundation), and meteorological conditions (rainfall) interact in a nonlinear manner to amplify flood risk. The sharp increase in inundation extent observed in 2026, following the minimum inundation recorded in 2025, suggests that the spatial resilience of coastal systems is not static. Rather, it is governed by a dynamic functional threshold, whereby the effectiveness of coastal protection infrastructure and natural environmental capacity can be exceeded under the cumulative influence of multiple interacting environmental stressors. This finding provides additional theoretical support for dynamic, process-based assessments of coastal flood vulnerability, rather than static evaluations based on individual hazard drivers alone.

Practical implications

From a practical perspective, the High and Very High vulnerability zonation maps produced using the CMA model can be directly adopted by the Pekalongan City Government as a primary reference for revising the Regional Spatial Plan and the Detailed Spatial for coastal areas. Based on these findings, tidal flood management in Pekalongan City should be integrated into a comprehensive and adaptive coastal management strategy. The predominance of land subsidence as the highest-weighted parameter highlights the urgent need to strengthen regulations governing deep groundwater extraction by the industrial sector while restricting permits for new heavy infrastructure development, particularly in Pekalongan Utara District. Stricter spatial planning policies are required to limit the conversion of wetlands and regulate industrial groundwater extraction in order to reduce the rate of land subsidence.

Operationally, the observed year-to-year fluctuations in inundation extent provide valuable guidance for prioritizing regional disaster mitigation investments. The significant reduction in flooding along the northernmost coastline of Pekalongan demonstrates the effectiveness of the coastal seawall system. Conversely, the persistence of chronic flooding in southern Pekalongan Utara and Pekalongan Barat indicates that future infrastructure investments should prioritize the rehabilitation of floodgates and the reinforcement of embankments along major river corridors. Specifically, the local government should prioritize the complete rehabilitation of the Meduri River embankment in Pekalongan Barat to reduce tidal overflow. This effort should be complemented by the modernization of the urban micro-drainage system through sediment dredging, together with the construction of interconnected drainage channels linked to the main polder system to prevent prolonged water retention within the Pekalongan basin.

Given the finite capacity of structural flood-control infrastructure, greater emphasis should also be placed on non-structural mitigation measures, including large-scale mangrove restoration and community-based dissemination of evacuation routes derived from the CMA vulnerability map to enhance public preparedness. In addition, the resulting vulnerability map provides an evidence-based planning tool for the Regional Disaster Management Agency to design early warning systems, establish appropriate evacuation routes, and strengthen community adaptive capacity according to the spatial characteristics of flood vulnerability.

Study limitations

Although the spatial modeling results demonstrate strong agreement with field observations, several technical limitations should be acknowledged. First, the 10-m spatial resolution of Sentinel-1 SAR imagery limits its ability to detect small-scale tidal inundation occurring within narrow residential alleys or areas obscured by dense urban vegetation canopies. Second, the annual rainfall data derived from the CHIRPS dataset provide information at a relatively coarse spatial scale, making them less capable of capturing localized short-term rainfall anomalies with high precision. Finally, land subsidence was modeled using mean annual deformation rates and therefore does not account for short-term temporal fluctuations associated with seasonal variations in surface loading. To ensure methodological rigor, the uncertainties associated with input data and spatial resolution were evaluated. The primary sources of uncertainty stem from the 10-m spatial resolution of Sentinel-1 SAR imagery in dense urban canopies, coarse CHIRPS precipitation grids, and temporal interpolation of land subsidence rates. Furthermore, while the current validation relies on empirical field verification points, future iterations of this framework would benefit from comparative sensitivity analyses against alternative statistical models to further quantify model variance and robustness.

To address these limitations in future research, the use of high-resolution elevation datasets, such as LiDAR, is recommended to improve the representation of micro-topographic variations in densely populated urban areas. Future studies should also integrate the CMA framework with IPCC climate projections and two-dimensional hydrodynamic modeling to simulate future tidal flood inundation under projected climate conditions through 2050.

Although model verification relied on a dedicated terrestrial dataset, the initial field sampling ($n = 30$) was strategically executed using a purposive framework focused primarily on active inundation sectors, urban residential zones, and critical flood channels to verify contemporary flood footprints (Foody, 2002; Congalton and Green, 2019). To evaluate multi-class vulnerability performance across all risk tiers without calibration bias, a balanced subset ($n = 20$) stratified across all five vulnerability classes was derived. Nevertheless, a methodological limitation of this study is the constrained sample size across non-flooded peripheral sectors. Future research should incorporate expanded spatial sampling grids and systematic random sampling designs across wider non-flooded control zones to further constrain localized uncertainty bounds and perform continuous spatial sensitivity matrix evaluations.

CONCLUSIONS

The findings of this study indicate that the objective CMA framework provides a data-driven approach for characterizing contemporary tidal flood vulnerability in Pekalongan City by integrating multi-temporal inundation observations with key environmental drivers. The results support the hypothesis that tidal flooding in low-lying coastal urban areas is controlled not only by marine exposure but also by interacting geological and hydrological factors. Based on the CMA matrix calculations, land subsidence was identified as the dominant controlling factor, receiving the highest parameter weight (24.49%), followed by Coastline buffer (21.98%) and River buffer (12.68%), confirming the critical role of ground deformation and hydraulic connectivity in amplifying coastal flood impacts.

The spatiotemporal analysis revealed that observed tidal flood inundation exhibited substantial temporal variability during 2022–2026, with a cumulative flood footprint of 810 ha, representing 17.54% of the total study area. Spatially, areas classified as High vulnerability (370.52 ha) and Very High vulnerability (541.12 ha) were concentrated in the northern and western parts of the city, with Pekalongan Utara District identified as the most vulnerable area. Ground-truth validation demonstrated a very high level of agreement between the CMA model and actual field conditions. Specifically, Tirto Village experienced the most severe impacts, with floodwaters persisting for up to 10 days because of damage to the Meduri River embankment, whereas Panjang Baru Village exhibited a marked reduction in flood occurrence following the operation of the coastal seawall in 2022. These findings provide new evidence that coastal flood vulnerability cannot be adequately explained by elevation or coastal distance alone but requires an integrated assessment of multiple interacting environmental processes.

This study contributes to filling the gap between static coastal flood susceptibility mapping and observation-based dynamic vulnerability assessment by incorporating empirically derived flood footprints into an objective weighting framework. Furthermore, benchmarking against the traditional AHP method confirmed a +10.00% improvement in predictive accuracy, demonstrating that empirical data-driven weighting offers a superior alternative for coastal hazard mapping. The selection of the 2022–2026 observation period proved appropriate for generating a contemporary flood vulnerability map that accurately reflects current conditions while minimizing overestimation bias arising from major structural interventions. However, the general applicability of the proposed model requires further verification through larger validation datasets, longer observation periods, and comparison with alternative statistical or machine-learning approaches.

REFERENCES

1. Hapsoro, A. W., and Buchori, I. (2015). Kajian kerentanan sosial dan ekonomi terhadap bencana banjir (studi kasus: wilayah pesisir kota Pekalongan), *Teknik PWK (Perencanaan Wilayah Kota), 4*(4), 542–553. https://doi.org/10.14710/tpwk.2015.9814
2. Al-Omari, A. A., Shatnawi, N. N., Shbeeb, N. I., Istrati, D., Lagaros, N. D., Abdalla, K. M. (2024). Utilizing remote sensing and GIS techniques for flood hazard mapping and risk assessment. *Civil Engineering Journal, 10*(5), 1423–1436. https://doi.org/10.1007/s12205-016-0019-m
3. Atkinson, P. M. (2013). Downscaling in remote sensing. *International Journal of Applied Earth Observation and Geoinformation*, *22*, 106–114. 10.1016/j.jag.2012.04.012
4. Bale, D. (Ed.). (1994). *Analisis pola pemukiman di lingkungan perairan di Indonesia.* Direktorat Jenderal Kebudayaan. https://short-url.cc/1B5Ub
5. Breiman, L. (2001). Random forests. *Machine Learning*, *45*(1), 5–32. https://doi.org/10.1023/A:1010933404324
6. Brommer, M. B., Bochev-van der Burgh, L. M. (2009). Sustainable coastal zone management: a concept for forecasting long-term and large-scale coastal evolution. *Journal of Coastal Research, 25*(1), 181-188. https://doi.org/10.2112/07-0909.1
7. Budiarto, F. A., Bioresita, F. (2023). Pemanfaatan citra Sentinel-1 SAR dan metode change detection approach untuk analisis sebaran spasial wilayah banjir dan Area Terdampak (studi kasus: banjir kabupaten Aceh utara 2022). *JGISE: Journal of Geospatial Information Science and Engineering, 6*(2), 153–162. https://doi.org/10.22146/jgise.87585
8. Bunga, B. A. R., Barus, B., Baskoro, D. P. T., Almismary, M. F. D. (2025). Estimasi populasi terpapar pada kejadian banjir di kecamatan Biringkanaya kota Makassar. *Jurnal Ilmu Lingkungan, 23*(3), 820–829. https://doi.org/10.14710/jil.23.3.820-829
9. Cao, A., Esteban, M., Valenzuela, V. P. B., Onuki, M.,

Takagi, H., Thao, N. D., Tsuchiya, N. (2021). Future of Asian Deltaic Megacities under sea level rise and land subsidence: Current adaptation pathways for Tokyo, Jakarta, Manila, and Ho Chi Minh City. *Current Opinion in Environmental Sustainability, 50*, 87-97. https://doi.org/10.1016/j.cosust.2021.02.010

10. Chen, Y., Yu, J., Khan, S. (2010). Spatial sensitivity analysis of multi-criteria weights in GIS-based land suitability evaluation. *Environmental Modelling & Software*, *25*(12), 1582–1591. https://doi.org/10.1016/j.envsoft.2010.06.001
11. Congalton, R. G. (1991). A review of assessing the accuracy of classifications of remotely sensed data. *Remote sensing of environment*, *37*(1), 35–46. https://doi.org/10.1016/0034-4257(91)90048-B
12. Congalton, R. G., Green, K. (2008). *Assessing the accuracy of remotely sensed data: principles and practices*. CRC press. https://short-url.cc/1B5Uf
13. DeVries, B., Huang, C., Armston, J., Huang, W., Jones, J. W., Lang, M. W. (2020). Rapid and robust monitoring of flood events using Sentinel-1 and Landsat data on the Google Earth Engine. *Remote sensing of Environment*, *240*, 111664. https://doi.org/10.1016/j.rse.2020.111664
14. Dewi, M., Syahra, Y. (2025). Implementasi sistem pendukung keputusan berbasis IOT dengan metode topsis untuk peringatan dini potensi bencana banjir. *Jurnal Komputer Teknologi Informasi Sistem Informasi (JUKTISI), 4*(2), 1133–1144. https://doi.org/10.62712/juktisi.v4i2.564
15. Egaputra, A. A., Ismunarti, D. H., Pranowo, W. S. (2022). Inventarisasi kejadian banjir rob kota Semarang periode 2012–2020. *Indonesian Journal of Oceanography, 4*(2), 29–40. https://doi.org/10.14710/jekk.v%25vi%25i.13240
16. Erkamim, M., Mukhlis, I. R., Putra, P., Adiwarman, M., Rassarandi, F. D., Rumata, N. A.,..., Hermawan, E. (2023). Sistem Informasi Geografis (SIG): Teori Komprehensif SIG. PT. *Green Pustaka Indonesia*. https://short-url.cc/1B5Uh
17. Feizizadeh, B., Blaschke, T. (2013). GIS-multicriteria decision analysis for landslide susceptibility mapping: comparing three different fuzzy analytical hierarchy process approaches and sensitivity analysis. *Natural Hazards*, *67*(2), 667–697. https://doi.org/10.1007/s11069-012-0463-3
18. Feizizadeh, B., Blaschke, T. (2013). GIS-multicriteria decision analysis for landslide susceptibility mapping: comparing three methods for the Urmia lake basin, Iran. *Natural hazards*, *65*(3), 2105–2128. https://doi.org/10.1007/s11069-012-0463-3
19. Foody, G. M. (2002). Status of land cover classification accuracy assessment. *Remote sensing of environment*, *80*(1), 185–201. https://doi.org/10.1016/S0034-4257(01)00295-4
20. Hudoyo, S. (2006). *Pengaruh Perkembangan Pendapatan Nelayan Terhadap Kondisi Fisik Permukiman Nelayan Wilayah Pesisir Kota Pekalongan* (Doctoral dissertation, Universitas Diponegoro). https://eprints.undip.ac.id/5014/
21. Hutabarat, L. E. (2017). *Studi Penurunan Muka Tanah (Land Subsidence) Akibat Pengambilan Air Tanah Berlebihan Di DKI Jakarta.* Kumpulan Karya Ilmiah Dosen Universitas Kristen Indonesia, 360–374. http://repository.uki.ac.id/id/eprint/904
22. Ibrahim, M., Purnaweni, H., Aqila, A., Wulandari, D., Kismartini, K., Djumiarti, T.,..., Amelia, S. (2024). Serious Flooding in Pekalongan City: What are the Government Policies in Tackling this Problem?. In *Proceedings of the 1st International Conference on Environmental Science, Development, and Management, ICESDM 2023*. https://doi.org/10.1051/e3sconf/202020206027
23. Ismanto, K., Pratikwo, S., Madusari, B. D., Christianto, P. A. (2021). Analisis kebutuhan masyarakat terdampak banjir rob: Studi kasus kota Pekalongan. *Jurnal Litbang Kota Pekalongan, 19*(1). https://short-url.cc/1vsq5
24. Jabbar, K. N. A., Handiani, D. N. (2023). Identifikasi sebaran banjir ROB pada kawasan pesisir di kabupaten subang dengan menggunakan Google Earth Engine. *Prosiding FTSP Series,* 952–957. https://eproceeding.itenas.ac.id/index.php/ftsp/article/view/2454
25. Jensen, J. R. (1996). *Introductory digital image processing: a remote sensing perspective.* 2nd Edition, Prentice Hall, Inc., Upper Saddle River, NJ. https://www.cabidigitallibrary.org/doi/full/10.5555/20001911540
26. Judijanto, L., Wibowo, G. A., Karimuddin, K., Samsuddin, H., Patahuddin, A., Anggraeni, A. F.,..., Simorangkir, F. M. A. (2024). *Research design: Pendekatan kualitatif dan kuantitatif*. PT. Sonpedia Publishing Indonesia. https://short-url.cc/1B5UW
27. Juwono, P. T., Subagiyo, A. (2017). *Ruang Air dan Tata Ruang: Pendekatan teknis keairan dan pembangunan berkelanjutan dalam penanganan banjir perkotaan*. Universitas Brawijaya Press. https://short-url.cc/1B5Va
28. Kasanah, N. (2020). Analisis lahan sawah tergenang banjir menggunakan metode change detection dan Pppm (phenology and pixel based paddy rice mapping)(studi kasus: Kabupaten Demak). *Jurnal Geodesi Undip, 10*(1), 259–268. https://doi.org/10.14710/jgundip.2021.29713
29. Koenawan, C. J., Zulfikar, A. (2025). Analisis risiko banjir rob dan kerentanan pesisir di kabupaten kepulauan anambas. *Jurnal Akuatiklestari, 9*(1), 33–38. https://doi.org/10.31629/akuatiklestari.v9i1.7698
30. Lasaiba, M. (2023). Analisis multikriteria berbasis sistem informasi geografis (SIG) terhadap bahaya dan resiko banjir di kecamatan sirimau kota ambon. *Jurnal Geosains Dan Remote Sensing, 4*(2),

77–90. https://doi.org/10.23960/jgrs.ft.unila.146

31. Lodwick, W. A., Monson, W., Svoboda, L. (1990). Attribute error and sensitivity analysis of map operations in geographical information systems: analysis of footprint definition. *International Journal of Geographical Information Systems*, *4*(4), 413–428. https://doi.org/10.1080/02693799008941556
32. Malczewski, J., Rinner, C. (2015). *Multicriteria decision analysis in geographic information science* (Vol. 1, pp. 55-77). New York: Springer. https://link.springer.com/book/10.1007/978-3-540-74757-4
33. Malik, A. A. M., Woy, V. T., Sela, R. L. E., Moniaga, I. (2023). Pengaruh kerapatan vegetasi dan kerapatan bangunan terhadap bencana banjir dan longsor di area perkotaan. *ARTEKS: Jurnal Teknik Arsitektur, 8*(2), 229–242. https://doi.org/10.30822/arteks.v8i2.2064
34. Millimono, T. S. (2026). Risk Production and urban vulnerability in conakry: Integrating governance, land use, and biophysical factors in the 2025 Manéah Landslide. *Trends in Ecological and Indoor Environmental Engineering (TEIEE)*, *4*(2), 44–59. https://doi.org/10.62622/TEIEE.026.4.2.44-59
35. Mutiarawati, T., Sudarmo, S. (2021). Collaborative governance dalam penanganan rob di Kelurahan Bandengan Kota Pekalongan. *Jurnal Mahasiswa Wacana Publik, 1*(1), 82–98. https://doi.org/10.20961/wp.v1i1.50892
36. Muttaqin, K., Maulita, M., Fitria, L., Ihsan, A., Mulya, R. (2023). mapping flood-prone areas based geographic information system using composite mapping analysis. *International Journal of Geoinformatics, 19*(12). https://doi.org/10.52939/ijg.v19i12.2983
37. Odiana, S., Yusuf, D. D. (2026). Time series modelling and forecasting of temperature and rainfall in nigeria using ARIMA models. *Trends in Ecological and Indoor Environmental Engineering*. *4*(3), 17–27. https://doi.org/10.62622/TEIEE.026.4.3.17-27
38. Oladosu, M. A., Abah, M. A., Odimgbe, E. I., Adewale, F. E., Arthur, C., Ajayi, A. S.,..., Ohanele, E. C. (2026). Smart electrochemical sensors and IoT for monitoring heavy metals in Nigerian water: review of advances and deployment challenges. *Trends in Ecological and Indoor Environmental Engineering*, *4*(1), 79–89. https://doi.org/10.62622/TEIEE.026.4.1.79-89
39. Olofsson, P., Foody, G. M., Herold, M., Stehman, S. V., Woodcock, C. E., Wulder, M. A. (2014). Good practices for estimating area and assessing accuracy of land change. *Remote sensing of Environment*, *148*, 42–57. https://doi.org/10.1016/j.rse.2014.02.015
40. Pande, C. B. (2022). Land use/land cover and change detection mapping in Rahuri watershed area (MS), India using the google earth engine and machine learning approach. *Geocarto International, 37*(26), 13860–13880. https://doi.org/10.1080/10106049.2022.2086622
41. Pratama, M. B. (2019, November). Tidal flood in Pekalongan: utilizing and operating open resources for modelling. In *IOP Conference Series: Materials Science and Engineering* (Vol. 676, No. 1, p. 012029). IOP Publishing. https://doi.org/10.1088/1757-899X/676/1/012029
42. Putra, D. R., Marfai, M. A. (2012). Identifikasi dampak banjir genangan (Rob) terhadap lingkungan permukiman di kecamatan Pademangan Jakarta Utara. *Jurnal Bumi Indonesia, 1*(1). https://short-url.cc/1B5Wf
43. Putro, S., Hayati, R. (2007). Dampak perkembangan permukiman terhadap perluasan banjir genangan di kota Semarang. *Jurnal Geografi: Media Informasi Pengembangan dan Profesi Kegeografian, 4*(1). https://short-url.cc/1B5Wr
44. Putro, S., Hariyanto, A. A., Amira, M. T. (2024). Efforts to increase the capacity of sukorejo village, semarang city community in facing landslide disasters through the preparation of evacuation standard operating procedures (SOPs). *Social Science and Humanities Journal.* https://doi.org/10.47006/.v6i2.788
45. Putro, S., Purnomo, S. H., Sriyono, S. (2021). Studi eksplorasi potensi pantai Dasun sebagai destinasi wisata di kecamatan Lasem kabupaten Rembang. *Edu Geography, 9*(2), 144–151. https://journal.unnes.ac.id/sju/index.php/edugeo/article/view/48777/19660
46. Putro, S., Purwoko, A., Sunarko, S. (2015). Pengaruh pengetahuan dan sikap tentang resiko bencana banjir terhadap kesiapsiagaan remaja usia 15–18 tahun dalam menghadapi bencana banjir di kelurahan Pedurungan Kidul kota Semarang. *Jurnal Geografi: Media Informasi Pengembangan Dan Profesi Kegeografian, 12*(2), 214–221. https://short-url.cc/1vssl
47. Ran, Q., Fu, W., Liu, Y., Li, T., Shi, K., Sivakumar, B. (2018). Evaluation of quantitative precipitation predictions by ECMWF, CMA, and UKMO for flood forecasting: Application to two basins in China. *Natural Hazards Review, 19*(2), 05018003. https://doi.org/10.1061/(ASCE)NH.1527-6996.0000282
48. Revathi, S., Selvakumar, P., Manjunath, T. C., Murugaveni, S., Varun, P., Sivakumar, B. G. (2026). Deep learning models for land cover classification and change detection in coastal zones. in earth observation and deep learning for coastal monitoring, mapping, and management (pp. 27-52). *IGI Global Scientific Publishing*. https://doi.org/10.4018/979-8-3373-8872-4.ch002
49. Rizki, N. K. T. (2024). Deteksi penurunan muka tanah menggunakan metode DinSAR dengan data Sentinel 1-A (studi kasus: kota Pekalongan, Jawa Tengah, Tahun 2022–2023). *Prosiding FTSP Series,* 379–385. https://eproceeding.itenas.ac.id/index.php/ftsp/article/view/3619
50. Salim, M. A., Siswanto, A. B. (2021). Kajian penanganan dampak banjir kabupaten pekalongan. *Rang Teknik Journal, 4*(2), 295–303. https://doi.

org/10.31869/rtj.v4i2.2525

51. Saltelli, A., Ratto, M., Andres, T., Campolongo, F., Cariboni, J., Gatelli, D.,..., Tarantola, S. (2008). *Global sensitivity analysis: the primer*. John Wiley & Sons. https://books.google.co.id/books?id=wAssmt2vumgC&lpg=PR7&ots=VXAzNg9N-3&lr&hl=id&pg=PR7#v=onepage&q&f=false
52. Sarah, D., Soebowo, E., Satriyo, N. A. (2021). Review of the land subsidence hazard in pekalongan delta, central java: Insights from the subsurface. *Rudarsko-geološko-naftni zbornik, 36*(4). https://doi.org/10.17794/rgn.2021.4.13
53. Setyaningsih, W. (2021). Adaptasi masyarakat pesisir dalam menghadapi perubahan garis pantai di pesisir kecamatan sayung. *Geo-Image Journal, 10*(2), 164–174. https://journal.unnes.ac.id/sju/index.php/geoimage/article/view/48983/19749
54. Setyaningsih, W., Saputro, P. A., Indrayati, A., Kurniawan, E., Syifauddin, M., Wijaya, V., Mahat, H. (2024). Spatial-temporal distribution and vulnerability level of tidal flooding in the coastal city of Semarang. *International Journal of Safety & Security Engineering, 14*(5). https://doi.org/10.18280/ijsse.140527
55. Singh, G., Rawat, K. S. (2024). Mapping flooded areas utilizing Google Earth Engine and open SAR data: A comprehensive approach for disaster response. *Discover Geoscience*, *2*(1), 5. https://doi.org/10.1007/s44288-024-00006-4
56. Sriyono, S., Benardi, A. I., Putro, S., M. Nurropik, M. N., Yametis, J. V. G., Rahmajati, J. P. (2024). Kajian kesiapsiagaan masyarakat dalam menghadapi bencana banjir di kabupaten Demak. *Indonesian Journal of Conservation*, *13*(1), 42–49. https://doi.org/10.15294/ijc.v13i1.5406
57. Stehman, S. V. (2009). Sampling designs for accuracy assessment of land cover. *International journal of remote sensing*, *30*(20), 5243–5272. https://doi.org/10.1080/01431160903131000
58. Thammaboribal, P., Triapthti, N. K., Lipiloet, S. (2025). Using of analytical hierarchy process (AHP) in disaster management: a review of flooding and landslide susceptibility mapping. *International Journal of Geoinformatics*, *21*(4), 177–196. https://doi.org/10.52939/ijg.v21i4.4091
59. Triarso, I. (2012). Potensi dan peluang pengembangan usaha perikanan tangkap di Pantura Jawa Tengah. Saintek Perikanan: Indonesian *Journal of Fisheries Science and Technology, 8*(1), 65–73. https://doi.org/10.14710/presipitasi.v%vi%i.329-337
60. Twele, A., Cao, W., Plank, S., Martinis, S. (2016). Sentinel-1-based flood mapping: a fully automated processing chain. *International Journal of Remote Sensing*, *37*(13), 2990–3004. https://doi.org/10.1080/01431161.2016.1192304
61. Wahjoerini, W. (2020). Konsep perancangan di kawasan pesisir pantai Sari kota Pekalongan. *Indonesian Journal of Spatial Planning, 1*(1), 25–28. http://dx.doi.org/10.26623/ijsp.v1i1.1988
62. Wang, G., Li, P., Li, Z., Liu, J., Zhang, Y., Wang, H. (2024). InSAR and machine learning reveal new understanding of coastal subsidence risk in the Yellow River Delta, China. *Science of the Total Environment, 915*, 170203. https://doi.org/10.1016/j.scitotenv.2024.170203
63. Xiao, Y., Yi, S., Tang, Z. A. (2018). Spatially explicit multi-criteria analysis method on solving spatial heterogeneity problems for flood hazard assessment. *Water Resour Manage 32*, 3317–3335. https://doi.org/10.1007/s11269-018-1993-6